

Substrate-Free Self-Assembled SiO_x-Core Nanodots from Alkylalkoxysilane as a Multicolor Photoluminescence Source for Intravital Imaging

Pei-Ying Lin¹, Chiung-Wen Hsieh¹, Mei-Lang Kung^{1,2} and Shuchen Hsieh^{1,*}

¹Department of Chemistry and Center for Nanoscience and Nanotechnology, National Sun Yat-sen University, Kaohsiung, 80424, Taiwan

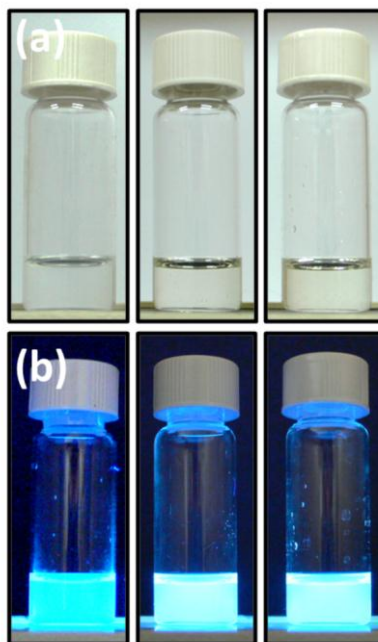
²Center of Neurobiology Science, National Sun Yat-sen University, Kaohsiung, 80424, Taiwan

*e-mail: shsieh@facmail.nsysu.edu.tw

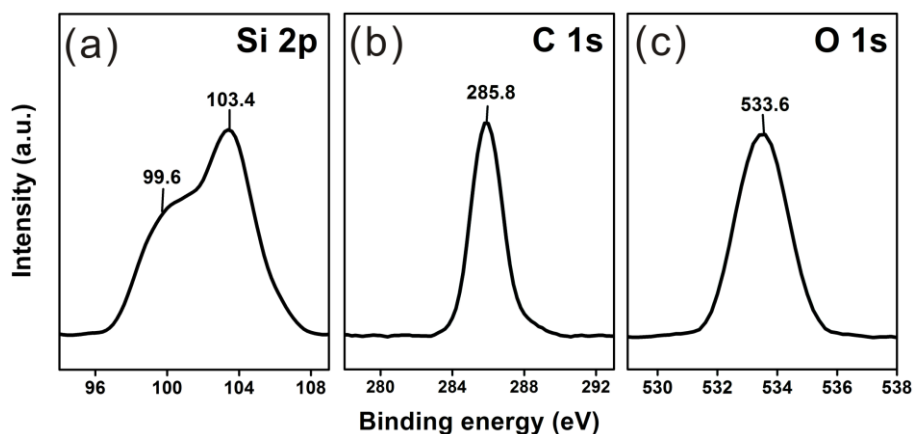
Table of contents

I. Supplementary Figures	S2
II. Supplementary References	S11

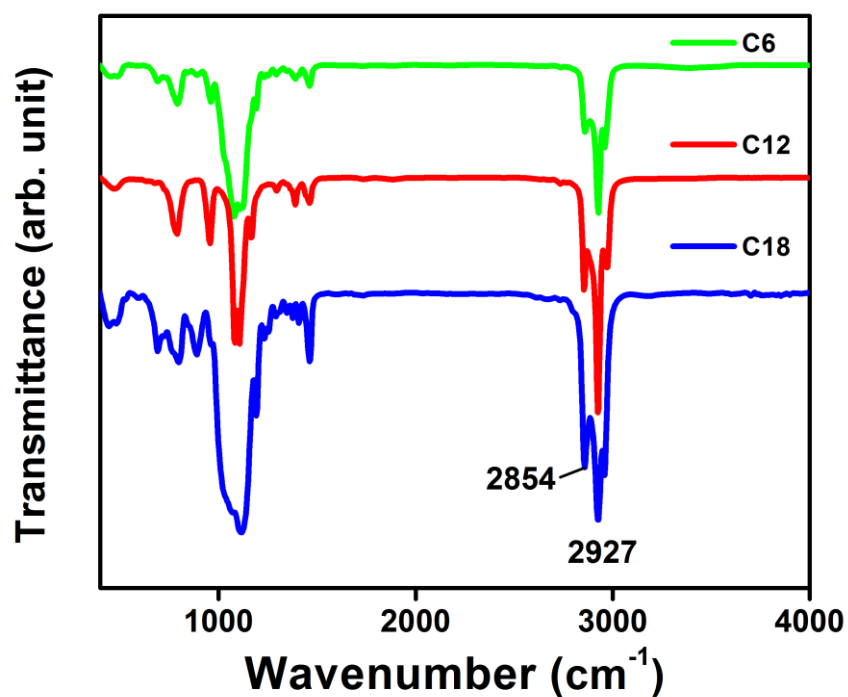
Supplementary Information



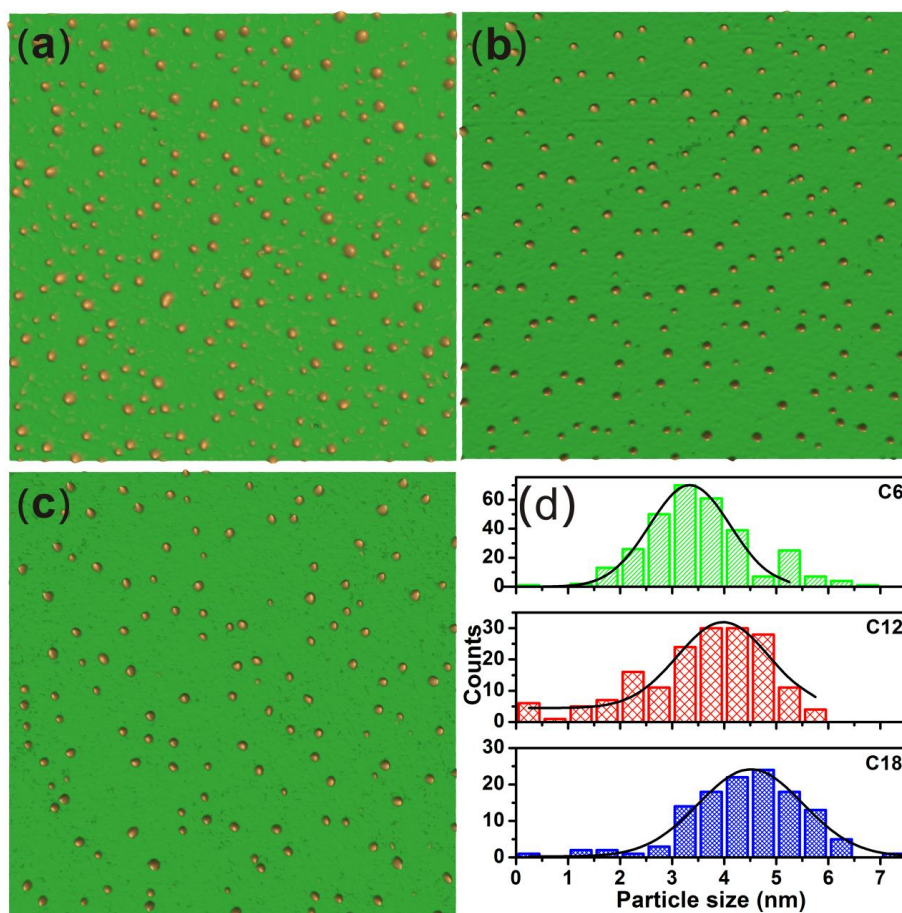
Supplementary Figure S1. Photographs of three types of SF-SAND. The images show the SF-SAND solutions of HTS (C6), DTS (C12), and OTS (C18) respectively, from *left to right*, before (a) and during exposure to (b) UV light irradiation at 365 nm.



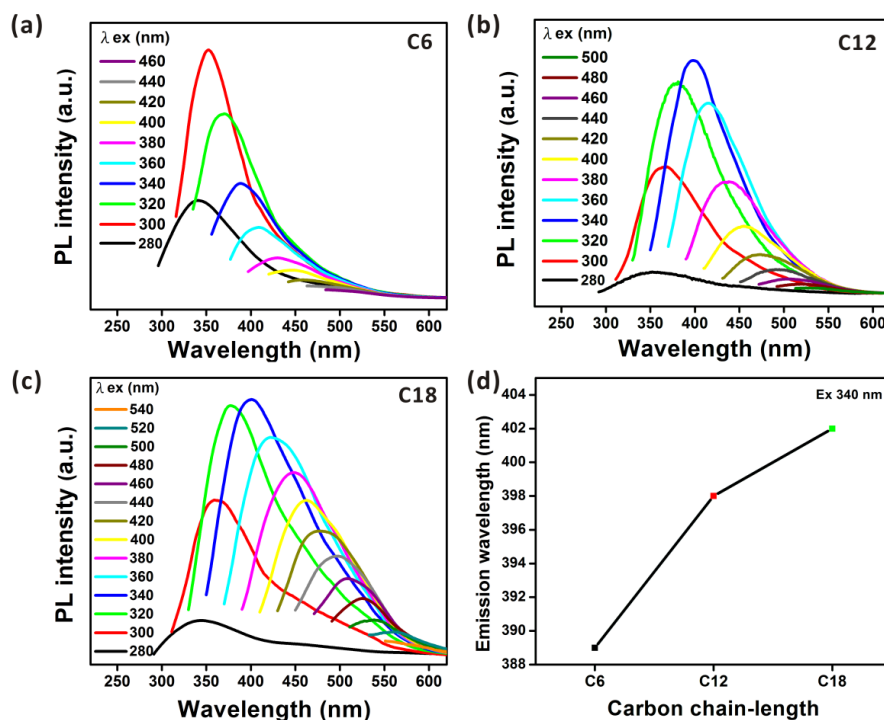
Supplementary Figure S2. XPS elemental peak positions for SF-SAND. The XPS data of SF-SAND deposited on gold showing (a) Si 2P, (b) C 1s, (c) O 1s binding energy peaks. The Si 2p peak at 103.4 eV represents SiO₂, and the lower binding energy peak at 99.6 eV indicates silicon. Figure (b) shows the C 1s spectrum with a binding energy peaked at 285.8 eV. This corresponds well to $-\text{CH}_2-$ carbon and confirms that the alkyl chains from the precursor are preserved in the NP product. Figure (c) shows the O 1s spectra at 533.6 eV which indicates a Si–O–Si bonding environment.



Supplementary Figure S3. FTIR spectra of SF-SAND derived from three types of alkylalkoxysilane. The as-prepared SF-SAND prepared from HTS (C6), DTS (C12), and OTS (C18), deposited on a silicon substrate. The peaks at 2854 and 2927 cm^{-1} correspond to the symmetric and anti-symmetric $-\text{CH}_2-$ stretching peaks, respectively, indicating the presence of alkyl groups. The intensity of $-\text{CH}_2-$ stretching peaks was consistent with the trend of increasing chain-length precursors.



Supplementary Figure S4. AFM topographical images ($2 \times 2 \mu\text{m}^2$) of SF-SAND deposited on silicon. (a-c) are corresponding to HTS (C6), DTS (C12), and OTS (C12), respectively, and (d) indicating height distribution histograms from nanoparticle analysis of images (a-c). The particle sizes of the SF-SANDs for C6, C12, and C18, were 3.36 ± 1.02 , 3.98 ± 1.22 , and 4.52 ± 1.09 nm, respectively. Sets of 306, 173, and 124 NPs were used in the statistical analysis.



Supplementary Figure S5. PL spectra from SF-SAND particles derived from three types of alkylalkoxysilane. Figure from (a) to (c) are HTS (C6), DTS (C12), and OTS (C18), respectively, and (d) shows that the corresponding fluorescence emission wavelengths from the three types of SF-SAND particles are 389 nm, 398 nm and 402 nm, respectively.

Quantum Yield Measurements

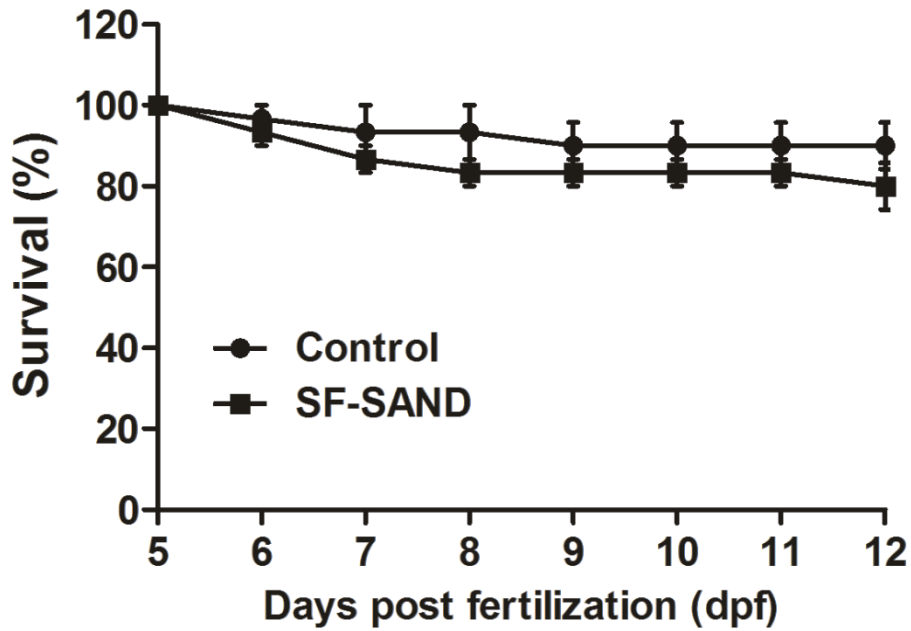
The quantum yield (QY) was estimated based on the experimental method described by Zhou *et al.*² Absolute QY values for the SF-SAND were calculated using a 0.1 M H₂SO₄ quinine sulfate standard reference sample that had a fixed and known fluorescence QY value (literature QY 54% at excited 340 nm). This method was used in that study to determine the QY of blue fluorescent carbon nanocrystals.

The quantum yield was calculated using the equation below:

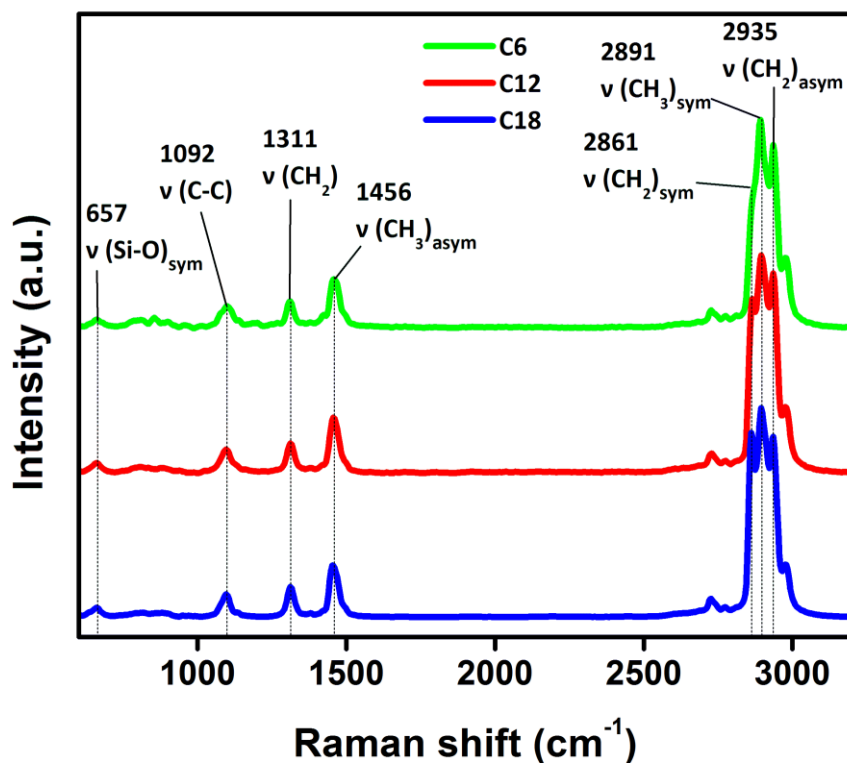
$$\varphi_x = \varphi_{std} \left(\frac{m_x}{m_{std}} \right) \left(\frac{\eta_x}{\eta_{std}} \right)^2$$

where φ is the quantum yield, m is slope, η is the refractive index of the solvent, the “ x ” indicates the unknown sample, and “ std ” refers to the quinine sulfate standard solution in 0.1 M H₂SO₄. Slope is the slope from the plot of integrated fluorescence intensity vs absorbance. The refractive index of the solvent was 1.333 for 0.1 M H₂SO₄, and the sample stock solutions were 1.408, 1.433 and 1.439 for HTS, DTS

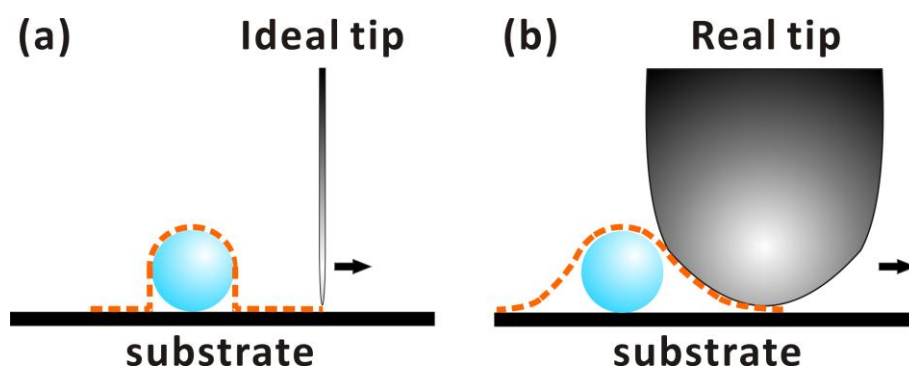
and OTS, respectively. Based on this reference, the QYs for the HTS, DTS and OTS derived SF-SAND samples were 3.1%, 28.8% and 45.6%, respectively.



Supplementary Figure S6. Effect of SF-SAND on zebrafish survival stress. Five days post fertilization (dpf) wild-type AB strains of *Danio rerio* (zebrafish) larvae were collected onto a petri dish before the experiment. SF-SAND material was mixed into the feed (9 in 1 ornamental fish pellet, AZOO, Taiwan) at an appropriate weight ratio of 1:1 (SF-SAND to feed). Triplicate experiments (n=10 Control/SF-SAND) were conducted to determine the effects of CDs on zebrafish larvae. Ninety minutes after zebrafish larvae were fed with SF-SAND feed (200 μ g of the SF-SAND/feed mixture was added into 200 μ l system water), the larvae were placed on the fluorescence microscope (Leica, DMIL, Germany) for intravital imaging (Fig. 4). Subsequently, for *in vivo* cytotoxicity measurements, larvae were transferred to a petri dish filled with system water and incubated at 28°C. The live larvae fish were monitored, counted, and recorded for 12 days post fertilization (dpf). As shown in Supplementary Fig. S6, the survival rate of the control and SF-SAND exposed zebrafish were 90 \pm 10% and 80 \pm 10%, respectively, demonstrating that there was no significant *in vivo* toxicity.



Supplementary Figure S7. Raman spectra of SF-SAND derived from three types of alkylalkoxysilanes. The as-prepared SF-SAND stock solutions prepared from HTS (C6), DTS (C12), and OTS (C18), were deposited on a silicon substrate. The peak at 657 cm^{-1} corresponds to a Si–O stretch. The peak at 1092 cm^{-1} corresponds to the C–C stretch. And, the peaks at 2861 and 2935 cm^{-1} correspond to the symmetric and anti-symmetric $-\text{CH}_2-$ stretching peaks, respectively, indicating the presence of alkyl groups.³



Supplementary Figure S8. Ideal (a) and real (b) AFM tip scan path.

If the AFM tip apex radius of curvature (ROC) is much smaller than the feature being imaged, the relatively sharp tip can precisely trace the profile of the feature (Figure S8a). However, if the ROC is comparable to or larger than the feature, then a lateral tip-broadening effect is observed. In such cases, as the tip scans over a particle (for example), the sides of the tip make contact with the particle before the true apex (Figure S8b) and the AFM responds. This leads to a lateral broadening of the apparent particle size in AFM images. Modern commercial AFM probe tips can be quite “sharp” with a radius of curvature on the order of $\sim 10\text{-}25$ nm or so or smaller. In our experiment, the particles were on the order of 4-5 nm, and the tip apex ROC likely 10-15 nm. Thus, depending on the actual ROC and tip shape, the apparent lateral particle size in our experiments could easily be >30 nm. Again, when using AFM to measure particle size, it is the height of the particle, not the apparent width that is used, because the AFM height measurement is not subject to this lateral tip-broadening effect.^{4,5}

Supplementary References

- 1 Cai, T., Wang, R., Neoh, K. G. & Kang, E. T. Functional poly(vinylidene fluoride) copolymer membranes via surface-initiated thiol-ene click reactions. *Polym. Chem.* **2**, 1849-1858 (2011).
- 2 Zhou, J. *et al.* An electrochemical avenue to blue luminescent nanocrystals from multiwalled carbon nanotubes (MWCNTs). *J. Am. Chem. Soc.* **129**, 744-745 (2007).
- 3 Shih, P. T. K. & Koenig, J. L. Raman studies of silane coupling agents. *Mater. Sci. Eng.* **20**, 145-154 (1975).
- 4 Lawn, M. A., Goreham, R. V., Herrmann, J. & Jämting, A. K. Particle number density gradient samples for nanoparticle metrology with atomic force microscopy. *Proc. SPIE* **8036**, 80360T-80360T-8 (2011).
- 5 Lv, Z., Wang, J., Chen, G. & Deng, L. Imaging recognition events between human IgG and rat anti-human IgG by atomic force microscopy. *Int. J. Biol. Macromol.* **47**, 661-667 (2010).